Journal of Inorganic and General Chemistry
ZAAC
Zeitschrift für anorganische und allgemeine Chemie
www.zaac.wiley-vch.de
RESEARCH ARTICLE

DOI: 10.1002/zaac.202200216

Mechanochemical synthesis and crystal structure evaluation of Na_2ZnSnS_4

Eva M. Heppke,[a] Thomas Bredow,[b] and Martin Lerch*[a]

Dedicated to Prof. Thomas Schleid on the occasion of his 65th birthday.

Phase-pure and highly crystalline Na_2ZnSnS_4 was prepared *via* a mechanochemical synthesis route. It crystallizes in the kesterite-type structure. The unusual large Debye-Waller factors of the sodium atoms were analyzed in detail, respecting also group-theoretical aspects. The results point to the existence of static disorder, mainly to the presence of various patterns of sodium ordering on a local scale. This is confirmed by quantum-chemical calculations at hybrid density-functional theory level. The dynamic atomic displacements due to phonons are much smaller than the observed Debye-Waller factors.

Introduction

$A_2^{I}B^{II}C^{IV}X_4^{VI}$ compounds have been in the focus of interest in recent years as they are known to be tunable semiconductors with a wide range of interesting properties.[1] Thereby, Cu_2ZnSnS_4 is currently one of the best-known representatives within this group and of technical interest as potential candidate as absorber material for thin film solar cells due to its optical band gap, high absorption coefficient, and its content of non-toxic and earth-abundant elements.[2] As reported by various research groups, 'doping' of Cu_2ZnSnS_4 with Na has a positive effect on the optical and, therefore, also on the photovoltaic properties of Cu_2ZnSnS_4.[3]

Formally, a total substitution of Cu by Na has just been achieved recently.[4] Not much literature is yet known about Na_2ZnSnS_4, but, however, according to the published articles[4,5] on synthesis, crystal structure, and properties of Na_2ZnSnS_4, it seems to crystallize in a chalcopyrite-derived crystal structure with an ordered arrangement of the cations[4] or the stannite-type structure,[5] both tetragonal, corresponding to Cu_2ZnSnS_4[6] and Cu_2FeSnS_4,[7] respectively. Both articles are primarily focused on the material properties of Na_2ZnSnS_4 such as optical, electronic, and electrical ones. In this regard, Na_2ZnSnS_4 was prepared either by a reactive flux method or a solid-state synthesis. For both synthesis routes, the desired product could only be obtained with large amounts of secondary phases; a completely phase-pure product could not be prepared. Consequently, the reflection intensities in the powder X-ray diffraction patterns of the published phases strongly deviate from the presented simulated ones. Interestingly, He et al.[4] picked a small single crystal out of their heterogenous reaction product (reactive flux method) and performed an X-ray single crystal structure analysis, suggesting a chalcopyrite-derived crystal structure. Taking a look at the reported cif-file, remarkable large anisotropic displacement parameters for the Na atoms are evident, indicating strong elongations along the tetragonal *c*-axis ($U_{33}/U_{11} \approx 5$). Unfortunately, this was not discussed or even mentioned in the article.

In the light of these results, we tried to realize the preparation of phase-pure Na_2ZnSnS_4 by applying mechanochemical synthesis techniques. On the basis of our experiences concerning the synthesis of sulfides of the type $A_2^{I}B^{II}C^{IV}X_4^{VI}$,[8] we developed a specific route optimized for the sodium-containing compound.

Results and Discussion

Na_2ZnSnS_4 was obtained as phase-pure and highly crystalline powder *via* a mechanochemical synthesis route described in the Experimental Section. The yellow/orange-colored powder of Na_2ZnSnS_4 is stable in air. The chemical composition was checked by energy dispersive X-ray spectroscopy (EDX) and agrees with the values from the chemical formula.

The observed reflections in the X-ray diffraction patterns of mechanochemically prepared samples of Na_2ZnSnS_4 indicate a tetragonal symmetry which fits to the proposed crystal structure types. Both the kesterite and stannite types are structurally derived from the chalcopyrite type.[6,9] All these crystal structures are built up by a cubic closest packing of

[a] Dr. E. M. Heppke, Prof. Dr. M. Lerch
Institut für Chemie
Technische Universität Berlin
Straße des 17. Juni 135, 10623 Berlin, Germany
E-mail: martin.lerch@tu-berlin.de
[b] Prof. Dr. T. Bredow
Mulliken Center for Theoretical Chemistry
Institut für Physikalische und Theoretische Chemie
Universität Bonn
Beringstraße 4, 53115 Bonn, Germany

Supporting information for this article is available on the WWW under https://doi.org/10.1002/zaac.202200216

sulfur anions with half of the tetrahedral voids filled with cations. The cation stacking sequences, though, differ. The stannite and kesterite types can be considered as typical structural representatives for quaternary $A_2^{I}B^{II}C^{IV}X_4^{VI}$ compounds, derived from cubic diamond-type structures, where alternating A^{I}- and B^{II}–C^{IV}-layers for stannite and A^{I}–B^{II}- and A^{I}–C^{IV}-layers for kesterite, stacked along the tetragonal *c*-axis, are present. In the chalcopyrite type, the B^{II} and C^{IV} cations are combined on one atomic position. This leads to a stacking of A^{I}–(B^{II}–C^{IV})-layers for quaternary $A_2^{I}B^{II}C^{IV}X_4^{VI}$ compounds adopting the chalcopyrite-type structure. The schematic visualization of these structure types is presented in Figure 1.

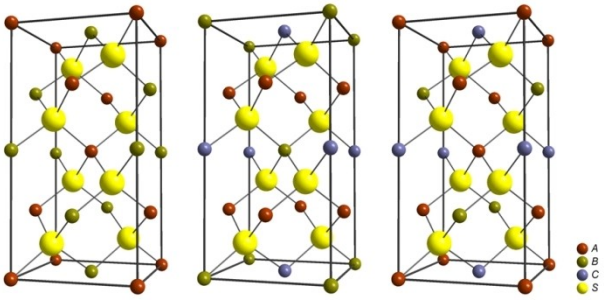

Figure 1. Crystal structures of the chalcopyrite (left), stannite (middle), and kesterite (right) type (red: A^{I}; green: B^{II}; blue: C^{IV}; yellow: S).

Table 1. Results of the Rietveld refinements for Na_2ZnSnS_4 in the chalcopyrite-, stannite-, and kesterite-type structure (standard deviations in parenthesis). Reliability factors have their established meaning.

Empirical formula	Na_2ZnSnS_4		
Structure type	chalcopyrite	stannite	kesterite
Space group	$I\bar{4}2d$	$I\bar{4}2m$	$I\bar{4}$
Crystal system	tetragonal	tetragonal	tetragonal
Z	2	2	2
a, Å	6.4762(7)	6.4789(15)	6.4876(3)
c, Å	9.1156(10)	9.121(2)	9.1327(4)
V, Å^3	382.32(7)	382.88(16)	384.38(2)
Calculated density, g/cm^3	3.112	3.108	3.096
Diffractometer	PANalytical X'Pert MDP Pro		
Radiation	Cu-K_α radiation		
Wavelength, Å	$\lambda_1 = 1.54056$, $\lambda_2 = 1.54439$		
R_p	0.068	0.142	0.0282
R_{wp}	0.102	0.222	0.0402
R_{exp}	0.0188	0.0189	0.0188
R_{Bragg}	0.195	0.384	0.0310
S (R_{wp}/R_{exp})	5.43	11.75	2.14

The crystal structure of Na_2ZnSnS_4 was refined using these three different structure models. As it can be clearly seen in Table 1, the kesterite-type is preferable (more details are presented in the Supporting Information: Tables S1 and S2, Figures S1 and S2). This is in good agreement with the results of He et al.[4] from their single crystal work, even though they did not use the name of this structure type. The atomic parameters of the refinement in the kesterite-type model are summarized in Table 2. Unusual high Debye-Waller factors of more than 5 Å^2 for the sodium atoms are most remarkable, but also the value for sulfur is large. It was not possible to refine the Debye-Waller factors for all atoms simultaneously. The values for zinc and tin were optimized by evaluating the effect of the particular values on the quality of the fit. All site occupation factors were fixed on the ideal values coming from the chemical composition. Test refinements with refined occupation factors for Na did not lead to significant deviations from the ideal values, pointing to no significant disorder for the cations. Figure 2 shows the powder X-ray diffraction pattern of mechanochemically prepared Na_2ZnSnS_4 with the results of the refinement in the kesterite-type structure (space group $I\bar{4}$). It is evident that the intensities of some reflections are not modeled sufficiently.

Comparing the unit cell of Na_2ZnSnS_4 with that of Cu_2ZnSnS_4 ($a = 5.427$ Å, $c = 10.87$ Å),[6] an extended *a*-axis and a shortened *c*-axis for Na_2ZnSnS_4 is obvious. Such a behavior has been observed for compounds crystallizing in so-called compressed chalcopyrite-like structures (usually space group $I\bar{4}2m$)[10] and is explained by the presence of a large cation (e.g. Ba, Pb, Eu). In Na_2ZnSnS_4, the altered lattice parameters in relation to those of Cu_2ZnSnS_4 are probably due to the larger ionic radius of Na^+ compared to those of the other cations (Zn^{2+} and Sn^{4+}).[11]

In the kesterite-type structure, all cations and anions are surrounded by four atoms leading to tetrahedral coordination. In Na_2ZnSnS_4, sulfur is surrounded by 1 Sn, 1 Zn, and 2 Na atoms. The polyhedra coordinating the individual cations, together with the refined bond lengths and angles, are depicted in Figure 3. All cation-sulfur distances are in good agreement with the values calculated from.[11,12] The refined angles show clear deviations from the ideal tetrahedral angle (see Figure 3). It should be mentioned that all distances and

Table 2. Refined atomic parameters for Na_2ZnSnS_4 in the kesterite-type structure (space group $I\bar{4}$, standard deviations in parenthesis).

Atom	Wyckoff	*x*	*y*	*z*	s.o.f	B_{iso}, Å^2
Na1	2*a*	0	0	0	1	5.5(4)
Na2	2*c*	0	$^1/_2$	$^1/_4$	1	5.6(2)
Zn	2*b*	$^1/_2$	$^1/_2$	0	1	1.2
Sn	2*d*	$^1/_2$	0	$^1/_4$	1	1.2
S	8 *g*	0.7613(11)	0.6998(6)	0.8871(5)	1	2.39(9)

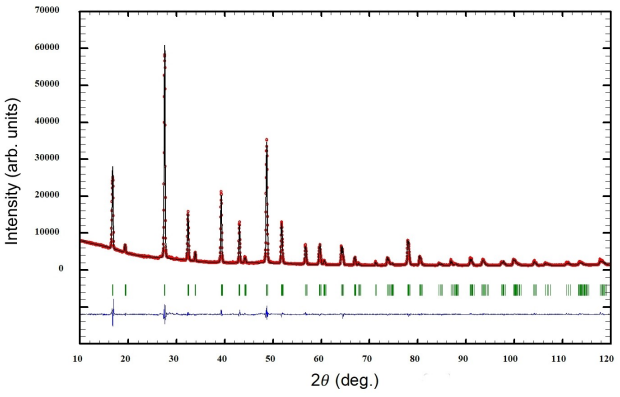

Figure 2. X-ray diffraction pattern of Na_2ZnSnS_4 with the results of the Rietveld refinement in the kesterite-type structure (space group $I\bar{4}$).

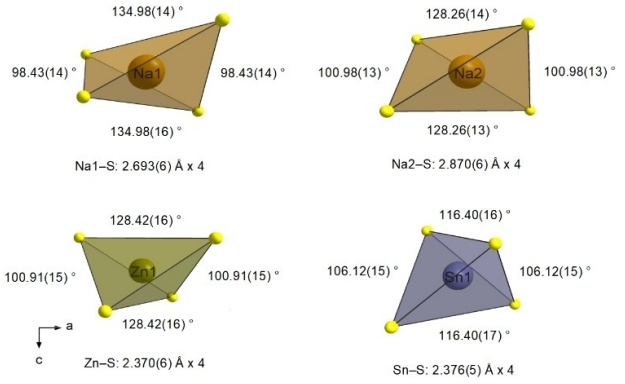

Figure 3. Coordination polyhedra around the cations in Na_2ZnSnS_4 with the determined sulfur-cation-sulfur angles and cation–sulfur bond lengths from the refinement in the kesterite-type structure (space group $I\bar{4}$).

Table 3. Results of the Rietveld refinements for Na_2ZnSnS_4 in the kesterite-type structure with refined anisotropic Debye-Waller factors (left), including split positions for the Na atoms (middle), and in the monoclinic space group *C*2 (standard deviations in parenthesis).

Empirical formula	Na_2ZnSnS_4		
Structure type	kesterite - *anisotropic*	kesterite - *split positions*	kesterite - *subgroup*
Space group	$I\bar{4}$	$I\bar{4}$	*C*2
Crystal system	tetragonal	tetragonal	monoclinic
Z	2	2	2
a, Å	6.4876(3)	6.4876(3)	9.1749(6)
b, Å			9.1325(4)
c, Å	9.1327(4)	9.1325(4)	6.4873(5)
β, °			134.999(4)
V, Å^3	384.39(3)	384.38(3)	384.37(4)
Calculated density, g/cm^3	3.096	3.096	3.096
Diffractometer	PANalytical X'Pert MDP Pro		
Radiation	Cu-K_α radiation		
Wavelength, Å	$\lambda_1 = 1.54056$, $\lambda_2 = 1.54439$		
R_p	0.0272	0.0271	0.0266
R_{wp}	0.0386	0.0385	0.0380
R_{exp}	0.0188	0.0188	0.0188
R_{Bragg}	0.0266	0.0258	0.0244
S (R_{wp}/R_{exp})	2.05	2.05	2.02

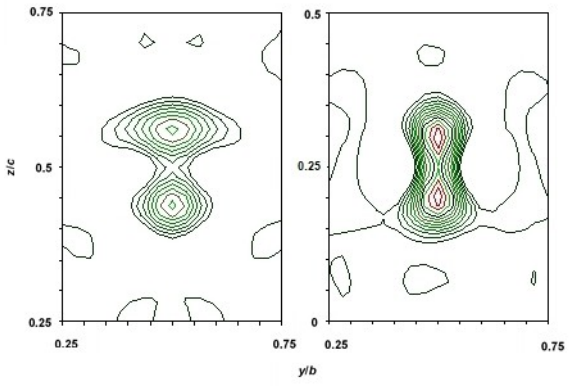

Figure 4. Difference Fourier maps for Na1 (left) and Na2 (right), calculated with the model using only isotropic contributions to the Debye-Waller factors (x(Na1) = $^1/_2$, (x(Na2) = 0). For reasons of clarity, only the contour lines between 0.9 and 1.5 e/Å^3 are presented.

angles are in accordance with those given by He et al.[4] (single crystal structure analysis).

In order to elucidate the origin of such unusual high Debye-Waller factors for sodium in more detail, the atomic displacements of both Na atoms were refined using a model allowing anisotropic contributions to the Debye-Waller factors. In good agreement with the single crystal work of He et al.,[4] severe elongations along the tetragonal *c* axis were observed. The residual values for this refinement are significantly better compared to those using isotropic Debye-Waller factors: R_{wp}-(iso) = 0.0402 → R_{wp}(aniso) = 0.0386; R_{Bragg}(iso) = 0.0310 → R_{Bragg}-(aniso) = 0.0266. More details are given in Table 3 and in the Supporting Information (Table S3 and Figure S3). These results point to the presence of dynamic (mobility of sodium) or static disorder.

The calculated difference Fourier maps, shown in Figure 4, clearly indicate the presence of two distinct maxima for Na near the ideal positions. In such a case, a model considering atoms on so-called split-positions is often helpful. In the standard model, presented in Table 2, Na atoms occupy the positions 0,0,0 and 0,1/2,1/4 (Wyckoff positions 2*a* and 2*c*, respectively). For the split model, respecting the results presented in Figure 4, the Na atoms occupy the positions 4*e* and 4*f*, respectively (0,0,z_1; 0,1/2,1/4 + z_2). As depicted in Table 4, the refined values are $z_1 = 0.025$; $z_2 = 0.037$, corresponding to shifts from the ideal positions of 0.23 and 0.34 Å, respectively. As the symmetry of the space group generates corresponding positions on the *c* axis with the same distance to the ideal values (0,0,-z_1; 0,1/2,1/4-z_2), the distance between the atoms on split positions are 0.46 (Na1) and 0.68 Å (Na2), respectively. As presented in Table 4, the Debye-Waller factors of both sodium atoms are significantly reduced compared to the standard model but always show

Table 4. Refined atomic parameters for Na_2ZnSnS_4 (space group $I\bar{4}$) introducing split positions for the Na atoms (standard deviations in parenthesis).

Atom	Wyckoff	*x*	*y*	*z*	s.o.f	B_{iso}, Å^2
Na1	4*e*	0	0	0.025(4)	0.5	3.4(4)
Na2	4*f*	0	1/2	0.2865(17)	0.5	2.5(3)
Zn	2*b*	1/2	1/2	0	1	1.2
Sn	2*d*	1/2	0	1/4	1	1.2
S	8*g*	0.7607(10)	0.6984(6)	0.8873(5)	1	2.04(9)

high values. The residual values for the model using sodium atoms on split positions are slightly better compared to the model respecting anisotropic contributions to the Debye-Waller factors (see Table 3). Figure 5 shows the powder X-ray diffraction pattern of Na_2ZnSnS_4 with the results of the refinement using the model with split positions. Comparing this difference curve with that presented in Figure 2 (isotropic Debye-Waller factors), a significant improvement is clearly observable.

In the light of these findings, another explanation of the unusual values of the Debye-Waller factors of the Na atoms should be discussed: keeping in mind the symmetry of space group $I\bar{4}$, compelling an equal distribution of the sodium atoms on the split positions, Na_2ZnSnS_4 may crystallize in a space group with lower symmetry and with an ordered distribution of sodium. Consequently, the maximal non-isomorphic subgroups were evaluated. There are *klassengleiche* ($2\times P\bar{4}$) and *translationengleiche* (*C*2) subgroups of index 2. The desired distribution of Na atoms (occupation of only one of the respective split positions) can only be achieved using the monoclinic space group *C*2. Consequently, the structural parameters for Na_2ZnSnS_4 were transformed from $I\bar{4}$ to *C*2. This is graphically explained in Figure 6, using the so-called Bärnighausen formalism.[13] Most important is the presence of two independent positions for each sodium atom, representing the split-positions of the model described above (Na1a, Na1b, Na2a, Na2b). In space group *C*2, it is possible to realize four different reasonable patterns of Na ordering (1a/2a, 1a/2b, 1b/2a, 1b/2b) with individually refinable positions for every Na atom.

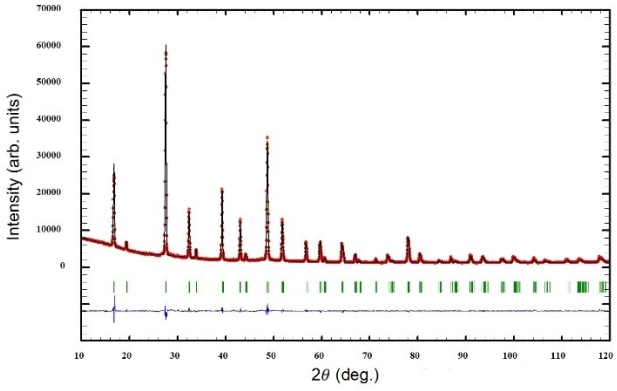

Figure 5. X-ray diffraction pattern of Na_2ZnSnS_4 with the results of the Rietveld refinement in the kesterite-type structure (space group $I\bar{4}$) introducing split positions for the Na atoms.

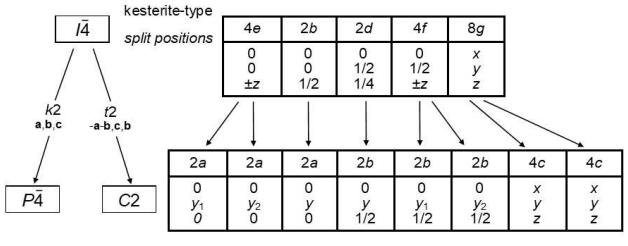

Figure 6. Group-theoretical relation (Bärnighausen formalism) between the kesterite-type structure including the split positions for the Na atoms and its maximal subgroups; description of the corresponding Wyckoff positions only for $I\bar{4}$ and *C*2.

As it can be seen in Table 3, the lattice parameters as well as the monoclinic angle were refined to values identical to the tetragonal ones within the standard deviations. Acting through the four ordering patterns described above, the resulting residual values are more or less the same and differ between 0.0382 and 0.0383 for R_{wp}, which is hardly mentionable superior to the best models with tetragonal symmetry. In a next step, a refinement with non-fixed occupation parameters for the sodium atoms were carried out (see also Supporting Information Figure S4). In order to avoid convergence problems, some of the parameters were not refined independently (see Table 5). The resulting shifts from the ideal positions in the simple tetragonal model are in the same range as those obtained from the above-described model using split positions. The distribution of sodium on the 'split positions' is not 1/2:1/2 (as in the tetragonal model) or 1:0 (as in the above described monoclinic models) but ~2/3:1/3 for both sodium atoms. Honestly, it should be stated that we are at the limit of powder X-ray methods with this. The resulting R_{wp}-value of 0.0380 is slightly better than the values presented above but, however, is not superior to the values obtained in test refinements using tetragonal symmetry with additional anisotropic Debye-Waller factors for the S atoms (keep in mind that there are two independent sulfur positions using the *C*2 model, Table 5).

Respecting the presented results, a monoclinic symmetry of the average crystal structure seems not to be reasonable. The refined lattice parameters, the monoclinic angle, and the atomic parameters point to a tetragonal symmetry. It should be mentioned that a monoclinic crystal structure (space group *C*2) was reported (X-ray single crystal structure analysis) for the

Table 5. Refined atomic parameters for Na_2ZnSnS_4 (space group *C*2, standard deviations in parenthesis).

Atom	Wyckoff	*x*	*y*	*z*	s.o.f	B_{iso}, Å^2
Na1a	2*a*	0	0.039(4)[§]	0	0.64(4)[§]	2.21(16)[§]
Na1b	2*a*	0	0.961(4)[§]	0	0.36(4)[§]	2.21(16)[§]
Na2a	2*b*	0	0.280(3)[§]	$^1/_2$	0.62(6)[§]	2.21(16)[§]
Na2b	2*b*	0	0.220(3)[§]	$^1/_2$	0.38(6)[§]	2.21(16)[§]
Zn	2a	0	0.5*	0	1	1.23(16)
Sn	2*b*	0	0.747(2)	$^1/_2$	1	1.51(9)
S1	4*c*	0.222(2)	0.8968(17)	0.9369(16)	1	0.83(15)[§]
S2	4*c*	0.6831(15)	0.129(2)	0.427(2)	1	0.83(15)[§]

*fixed *y* value (polar space group); [§]not refined independently.

corresponding Cd-containing sulfide Na_2CdSnS_4.[14] Unfortunately, the relationship to the kesterite type was not discussed by the authors, but it can be easily seen that small but significant deviations from the tetragonal symmetry are present (lattice parameters, monoclinic angle, atomic positions). The reported pattern of sodium order corresponds to 1a/2a in our model. Interestingly, the deviations of the Na atoms from the tetragonal symmetry are nearly the same as the values refined in our split model and our monoclinic model described above. This points to the local presence of all four patterns of ordering in Na_2ZnSnS_4 (1a/2a, 1a/2b, 1b/2a, 1b/2b), giving a tetragonal average crystal structure in the refinements.

In order to check the above-presented structural model derived from powder diffraction, and to investigate additional dynamical effects on the disorder of Na and S atoms, quantum-chemical calculations were performed. As a first step, five unit cells with space groups $I\bar{4}$ and *C*2 (Table 3) were optimized at PW1PW-D3 level. In the four *C2* structures, only two of the four Na sites shown in Table 5 are occupied (1a/2a, 1a/2b, 1b/2a, 1b/2b), as mentioned above. After full relaxation of lattice parameters and atomic coordinates within the respective space group symmetries, the lattice energies of the five structures were identical within numerical precision. The Na–S distances in the optimized unit cells with *C2* symmetry differed by 0.002–0.008 Å. The average Na1–S and Na2–S distances of all five unit cells are identical, 2.71 Å and 2.77 Å, respectively (exp. 2.69 Å and 2.87 Å, Figure 3). Also, the lattice parameters are close to the results of the Rietveld refinement (Table 3), e.g. $a = 9.16$ Å, $b = 9.10$ Å, $c = 6.42$ Å, $\beta = 135.5°$ for the unit cell with space group *C2* and Na occupying 1a/2b sites, and $a = 6.41$ Å, $b = 9.13$ Å for the unit cell with space group $I\bar{4}$. From these results we conclude that the five structural models obtained from powder diffraction are energetically equivalent and all contribute to the observed structure of mechanochemically prepared Na_2ZnSnS_4.

The covalent bonding between metal and S atoms was analyzed by means of the crystal orbital Hamilton population (COHP) (see Supporting Information Figure S5). Both Zn and Sn have strong bonding and antibonding contributions, while the covalent Na–S interaction is weakly repulsive, indicated by the negative COHP.

In principle, the experimentally observed displacements for the Na and S atoms can also be due to dynamic effects, e.g. lattice phonons. The normal modes of Na_2ZnSnS_4 were calculated for a conventional unit cell with $I\bar{4}$ symmetry. No imaginary modes were observed, which confirms this structure as a local minimum. The two lowest normal modes (no. 4 and 5, since the first three modes correspond to translations) have very low frequencies (10 and 16 cm^{-1}). These modes mainly correspond to displacements of the S atoms, see the calculated normal mode vectors and the projected phonon density of states in Figures 7 and S6 (Supporting Information), respectively. Modes no. 6 and 7 are slightly higher in energy (44 and 57 cm^{-1}, respectively), but can still be considered as soft modes which are readily excited even at room temperature. In these modes, essentially only Na atoms are displaced along the *c* direction. If these two modes are excited, the maxima of the probability density of the Na atoms will shift towards the boundaries of the potential curves shown in Figure 8. However, the maximum displacements at energies < 2 kJ/mol are one

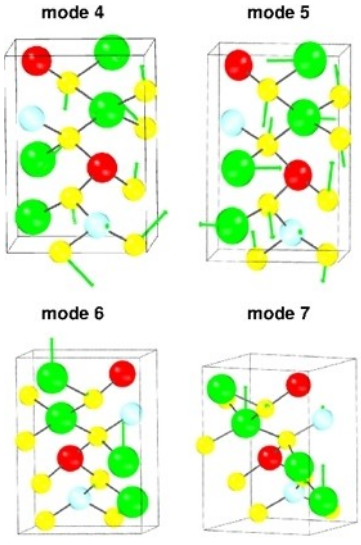

Figure 7. Displacement vectors of the first four calculated phonon modes of the conventional Na_2ZnSnS_4 unit cell with space group $I\bar{4}$. S atoms are yellow, Na atoms green, Sn red, and Zn light blue. The graphs were obtained with PDielec version 7.1.1.[15]

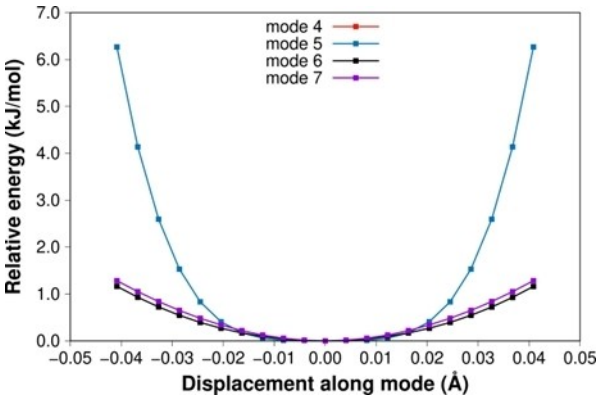

Figure 8. Potential curves for phonon modes 4–7 shown in Figure 7. The curves of modes 4 and 5 are almost identical.

order of magnitude smaller than the measured values (0.23 and 0.34 Å, for Na1 and Na2, respectively, see above). This energy threshold approximately corresponds to the thermal energy *RT* at room temperature. Due to the statistical energy distribution over all normal modes, the highest energy level of modes 4–7 will be even lower. Therefore, we conclude that dynamic effects play only a minor role for the large Debye-Waller factors of Na1 and Na2. The S atoms are dynamically displaced from their equilibrium positions as well, but the corresponding potential curves (Figure 8, the curves for modes 4 and 5 are almost identical) steeply increase for displacements larger than ±0.02 Å. Calculated anisotropic displacement parameters support the above analysis of the normal mode vectors. The Na atoms have large contributions in *z* direction, but also the S atoms have relatively large principal axis components along *z*. As outlined above, the computed atomic displacement parameters are much smaller than the refined ones, but they reproduce the experimental trends (a comparison is presented in Table S3, Supporting Information).

Conclusions

Phase-pure and highly crystalline Na_2ZnSnS_4 was prepared *via* a mechanochemical synthesis route. The presence of a kesterite-type crystal structure was made plausible from the results of powder X-ray diffraction methods incl. Rietveld refinements. Analyses of the unusually large Debye-Waller factors for the sodium atoms point to the existence of static disorder and the presence of lower symmetry on a local scale. The large ionic radius of Na^+, not fitting perfectly to the kesterite type (when zinc, tin, and sulfur are present) seems to be the main reason for this behavior, but also effects coming from the mechanochemical synthesis should be kept in mind.

Quantum-chemical calculations showed that structural models with tetragonal and monoclinic symmetry are energetically equivalent and will equally contribute to the crystal structure. Dynamic effects due to lattice phonons are too small to explain the Debye-Waller factors.

Powder X-ray methods are not the best choice for the analysis of atomic displacements in solids. Consequently, neutron diffraction experiments down to low temperatures will be carried out, which should also provide information concerning the presence of static disorder. To check possible twinning, we work on the preparation of single crystals.

Experimental Section

Synthesis

Na_2ZnSnS_4 was prepared *via* a mechanochemical synthesis route implying two synthesis steps for the preparation of multinary sulfides. In the first step, the corresponding binary sulfides Na_2S (Sigma Aldrich), ZnS, SnS, and additional sulfur (Fluka, 99.99%) were milled in a high energy planetary Mono Mill PULVERISETTE 6 (Fritsch, Idar-Oberstein, Germany) at a rotational speed of 350 rpm for five hours. Thereby, a 45 mL zirconia grinding beaker and six zirconia balls with a diameter of 15 mm were used. The second step of the synthesis procedure is the annealing of the milled powder at 723 K for two hours in H_2S atmosphere to increase its crystallinity. ZnS was synthesized by sulfidation of zinc oxide at 923 K for three hours in a tube furnace. SnS was prepared in evacuated and sealed SiO_2-ampoules by a solid-state reaction using tin (Merck, 99.9%) and sulfur (Fluka, 99.99%) as reactants.

Chemical and structural characterization

For powder X-ray diffraction measurements, a Panalytical X'Pert PRO diffractometer with nickel-filtered Cu-K_α radiation was used. The diffraction data was collected in a Bragg-Brentano setup at room temperature over an angular range of 10–120° with a step size of 0.026° and an exposure time of 60 s at each point. Additional measurements were carried out with a RIGAKU SmartLab 3 kW system equipped with a Kα_1 unit (Johansson-type Ge crystal, Cu-$K_{\alpha1}$ radiation, $\lambda = 1.54060$ Å). For Rietveld refinements[16] the program package FULLPROF Suite[17] was used. A pseudo-Voigt function was applied to fit the reflection profiles. Elemental analysis was carried out by means of energy dispersive X-ray spectroscopy (EDX) using a DSM 982 GEMINI spectrometer (Carl Zeiss AG, Oberkochen, Germany) equipped with an XFlash 6|60 detector (Bruker, Billerica, USA). The obtained values agree with the ideal ones from the chemical formula within two times the expected experimental error. All measurements were performed at the Zentrum für Elektronenmikroskopie (ZELMI) of TU Berlin (see also Figure S7 in the Supporting Information).

Quantum Chemical calculations

Energy calculations and crystal structure optimizations were performed with the crystalline orbital program CRYSTAL17[18] employing the PW1PW hybrid functional[19] and basis sets of triple-zeta plus polarization quality.[20] Long-range London dispersion effects were taken into account with the D3BJ correction[21] including three-body terms. The empirical s_8 parameter was adjusted to 1.5363 to obtain best agreement for calculated and measured lattice parameters. Strict truncation thresholds (10^{-7}, 10^{-7}, 10^{-7}, 10^{-14}, 10^{-42}) were applied for the calculation of two-electron integrals, as recommended for hybrid functionals. Integration in reciprocal space was performed with 4×4×4 Monkhorst-Pack grids. Crystal orbital Hamilton populations (COHP) were calculated with the algorithm implemented by Ruggiero et al.[22] Calculations of the projected phonon density of states applied the

method by Baima et al.[23] The anisotropic displacement parameters were calculated with the approach of Erba et al.[24]

Acknowledgements

This work was supported by the German Science Foundation – DFG (LE781/19-1, INST131/734-1 FUGG). Special thanks to the Zentrum für Elektronemikroskopie (ZELMI) of the TU Berlin giving access to EDX measurements, carried out by Dr. Stefan Berendts. Open Access funding enabled and organized by Projekt DEAL.

Conflict of Interest

The authors declare no conflict of interest.

Data Availability Statement

The data that support the findings of this study are available from the corresponding author upon reasonable request.

Keywords: quaternary sulfides · solar cell materials · mechanochemical synthesis · Rietveld refinement · quantum-chemical calculations

[1] a) M. Pandey, K. W. Jacobsen, *Phys. Rev. Mater.* **2018**, *2*, 105402/1–105402/12; b) S. Adachi, *Earth-abundant materials for solar cells: Cu_2-II–IV-VI_4 semiconductors*, John Wiley & Sons, Chichester, West Sussex, United Kingdom **2015**; c) C. Sevik, T. Çağın, *Phys. Rev. B* **2010**, *82*, 045202/1–045202/7; d) J. W. Lekse, M. A. Moreau, K. L. McNerny, J. Yeon, P. S. Halasyamani, J. A. Aitken, *Inorg. Chem.* **2009**, *48*, 7516–7518.

[2] a) K. Ito, T. Nakazawa, *Jpn. J. Appl. Phys.* **1988**, *27*, 2094–2097; b) H. Katagiri, K. Saitoh, T. Washio, H. Shinohara, T. Kurumadani, S. Miyajima, *Sol. Energy Mater. Sol. Cells* **2001**, *65*, 141–148; c) J. Seol, S. Lee, J. Lee, H. Nam, K. Kim, *Sol. Energy Mater. Sol. Cells* **2003**, *75*, 155–162; d) W. Wang, M. T. Winkler, O. Gunawan, T. Gokmen, T. K. Todorov, Y. Zhu, D. B. Mitzi, *Adv. Energy Mater.* **2014**, *4*, 1301465.

[3] a) M. Marzougi, M. Ben Rabeh, M. Kanzari, *Thin Solid Films* **2019**, *672*, 41–46; b) S. Berman, G. Sai Gautam, E. A. Carter, *ACS Sustainable Chem. Eng.* **2019**, *7*, 5792–5800; c) K. S. Gour, A. K. Yadav, O. P. Singh, V. N. Singh, *Vacuum* **2018**, *154*, 148–153.

[4] J. He, Y. Guo, W. Huang, X. Zhang, J. Yao, T. Zhai, F. Huang, *Inorg. Chem.* **2018**, *57*, 9918–9924.

[5] G. Bousselmi, N. Khemiri, A. Benali, M. P. F. Graca, R. F. Santos, B. F. O. Costa, M. Kanzari, *J. Mater. Sci. Mater. Electron.* **2020**, *31*, 18858–18869.

[6] S. R. Hall, J. T. Szymanski, J. M. Stewart, *Can. Mineral.* **1978**, *16*, 131–137.

[7] L. O. Brockway, *Z. Kristallogr.* **1934**, *89*, 434–441.

[8] a) A. Ritscher, J. Just, O. Dolotko, S. Schorr, M. Lerch, *J. Alloys Compd.* **2016**, *670*, 289–296; b) A. Ritscher, A. Franz, S. Schorr, M. Lerch, *J. Alloys Compd.* **2016**, *689*, 271–277; c) E. M. Heppke, T. Küllmey, I. Efthimiopoulos, F. D. Avci, O. Appelt, B. Paulus, M. Lerch, *Mater. Res. Express* **2019**, *6*, 125525; d) E. M. Heppke, S. Berendts, M. Lerch, *Z. Naturforsch.* **2020**, *B 75*, 393–402; e) E. M. Heppke, M. Lerch *Z. Naturforsch.* **2020**, *B 75*, 721–726; f) E. M. Heppke, S. Mahadevan, T. Bredow, M. Lerch, *Z. Naturforsch.* **2021**, *B 76* 607–614.

[9] S. Schorr, *Thin Solid Films* **2007**, *515*, 5985–5991.

[10] a) C. L. Teske, *Z. Naturforsch.* **1979**, *B 34*, 544–547; b) J. A. Aitken, P. Larson, S. D. Mahanti, M. G. Kanatzidis, *Chem. Mater.* **2001**, *13*, 4714–4721; c) S. S. Stoyko, A. J. Craig, J. W. Kotchey, J. A. Aitken, *Acta Crystallogr. Sect. C* **2021**, *77*, 1–10.

[11] B. Cordero, V. Gómez, A. E. Platero-Prats, M. Revés, J. Echeverría, E. Cremades, F. Barragán, S. Alvarez, *Dalton Trans.* **2008**, 2832–2838.

[12] P. Pykkö, *Phys. Rev. B* **2012**, *85(2)*, 024115–1-024115-7.

[13] a) H. Bärnighausen, *MATCH* **1980**, *9*, 139–175; b) U. Müller, *Z. Anorg. Allg. Chem.* **2004**, *630*, 1519–1537.

[14] M. S. Devi, K. Vidyasagar, *J. Chem. Soc. Dalton Trans.* **2002**, *9*, 2092–2096.

[15] J. Kendrick, A. D. Burnett, *J. Comput. Chem.* **2016**, *37*, 1491–1504.

[16] H. M. Rietveld, *J. Appl. Crystallogr.* **1969**, *2*, 65–71.

[17] J. Rodriguez-Carvajal, *Abstracts of the Satellite Meeting on Powder Diffraction of the XV. Congress of the IUCr* **1990**, 127.

[18] R. Dovesi, A. Erba, R. Orlando, C. M. Zicovich-Wilson, B. Civalleri, L. Maschio, M. Rérat, S. Casassa, J. Baima, S. Salustro, B. Kirtman, *Wiley Interdiscip. Rev.: Comput. Mol. Sci.* **2018**, *8*.

[19] T. Bredow, A. R. Gerson, *Phys. Rev. B* **2000**, *61*, 5194–5201.

[20] a) D. Vilela Oliveira, J. Laun, M. F. Peintinger, T. Bredow, *J. Comput. Chem.* **2019**, *40*, 2364–2376; b) J. Laun, T. Bredow, *J. Comput. Chem.* **2022**, *43*, 839–846.

[21] S. Grimme, S. Ehrlich, L. Goerigk, *J. Comput. Chem.* **2011**, *32*, 1456–1465.

[22] M. T. Ruggiero, A. Erba, R. Orlando, T. M. Korter, *Phys. Chem. Chem. Phys.* **2015**, *17*, 31023–31029.

[23] J. Baima, M. Ferrabone, R. Orlando, A. Erba, R. Dovesi, *Phys. Chem. Miner.* **2016**, *43*, 137–149.

[24] A. Erba, M. Ferrabone, R. Orlando, R. Dovesi, *J. Comput. Chem.* **2013**, *34*, 346–354.

Manuscript received: June 22, 2022
Revised manuscript received: August 15, 2022

